Disturbance Observer for Path-following Control of Autonomous Agricultural Vehicles

T. Hiramatsu, M. Pencelli, S. Morita, M. Niccolini, M. Ragaglia and A. Argiolas
Yanmar R&D Europe S. R. L., Viale Galileo 3/A, Firenze, Italy

Keywords: Path-following Control, Agricultural Tractor, Disturbance Observer.

Abstract: This paper proposes a disturbance observer to be integrated inside a path-following controller in order to improve motion accuracy of an autonomous driving tractor. During operation, the tractor undergoes the effects of external forces due to either the action of the implement or the inclination of the ground. In such conditions, it is difficult to work precisely along a pre-determined path. By considering external forces as disturbances, it is possible to design a disturbance observer that estimates the steering angle on the basis of yaw-rate and lateral velocity. The proposed approach has been tested in a simulation environment.

1 INTRODUCTION

With rises in global population comes the problem of food shortages. For instance, in Japan the number of farmers is decreasing and farmers are rapidly aging (Noguchi and Barawid, 2011). In the near future, this situation will likely result in shortages in food production. Eventually, the same issue is expected to happen all over the world (Blackmore, 2009), (Ball et al, 2017). For these reasons, automation technologies such as autonomous driving are needed to work large fields with fewer farmers. One of the most relevant problems in automated agriculture consists in controlling a machine along a predetermined path, in presence of rough terrain or inclined ground. Furthermore, the presence of ridges requires agriculture vehicles to move within 5.00-10.00 cm accuracy with respect to the predetermined path. Unfortunately, the presence of the implement and also the effect of gravity on inclined fields typically introduce disturbance effects that prevent the machine to achieve the required accuracy. Moreover, motion accuracy is influenced by soil conditions, which in turn depend on geographical location, climate and other environmental factors.

Even though, in principle, it would be possible to accurately model slip phenomena by taking into account all the aforementioned factors, the resulting model would almost surely be too complex to be used for control purposes. For this reason, rather than focusing on the physical modelling of these disturbances, the research community spent a significant effort in developing compensation strategies to overcome the effects of slip phenomena and to improve motion accuracy. Several solutions based on Kalman filtering have been proposed, like for instance (Shalal et al, 2013), (Pentzer et al, 2014), (Lenain et al, 2004), (Fang et al, 2005). Alternative approaches relying on both dynamic models and Kalman filtering proved to be effective in estimating slipping or, alternatively, in identifying the resulting variation of the instantaneous centre of rotation. However, the main limitation of these approaches consists in limited robustness with respect to rapidly changing soil conditions. More recently, techniques based on disturbance observation have been proposed to solve these problems, like for instance (Wen-Hua et al, 2016) and (Hyungbo et al, 2016). More in detail, the disturbance observer (DOB) consists in an inner-loop controller, whose primary role is just to compensate uncertainties in the plant and exogenous process disturbances. Several applications of DOB to the control of autonomous vehicles can be found in the scientific literature. For instance, in (Nguyen et al, 2014) the authors propose a DOB to estimate the vehicle's yaw angle using low-cost sensors. While being based on a rather simple kinematic car-like model, this solution is actually able to improve the controller's accuracy by reducing the lateral error with respect to the pre-defined path. In (Huang and Zhai, 2015), a DOB is applied to estimate exogenous disturbances acting on a wheeled mobile robot. In (Taghia and Katupitiya, 2013), a sliding mode controller is designed with DOB for a farm vehicle.

Hiramatsu, T., Pencelli, M., Morita, S., Niccolini, M., Ragaglia, M. and Argiolas, A.
Disturbance Observer for Path-following Control of Autonomous Agricultural Vehicles.
DOI: 10.5220/0007834402510258
In *Proceedings of the 16th International Conference on Informatics in Control, Automation and Robotics (ICINCO 2019)*, pages 251-258
ISBN: 978-989-758-380-3

The DOB eliminates the chattering of sliding mode control and compensates the system uncertainties. A different approach is proposed in (Rathgeber et al, 2015), where the authors face the problem of lateral trajectory tracking control of an autonomous driving car. A DOB-based controller that rejects external forces has been adopted in (Yu et al, 2018) in order to compensate the effect of cross-wind on the motion of a 4-wheel steering vehicle. However, this approach does not take into account the path-tracking problem and it also lacks versatility since it relies on extensive tuning of both controller and observer gains.

In this paper, we propose a DOB-based path-following control algorithm able to improve the accuracy of an autonomous agricultural tractor in terms of lateral error with respect to a pre-defined path. The external forces originating either from the action of the implement or from the inclined ground are directly considered as disturbances. The proposed DOB combines the yaw-rate and the lateral velocity of the vehicle to reject the exogenous disturbances. As a result, the main advantages of this approach consist in eliminating the need to re-tune control gains whenever soil conditions change. The remainder of the paper is structured as follows: Section 2 introduces the proposed control system, while Section 3 describes the adopted dynamic model, and the DOB's transfer function is analysed. Finally, simulation results are shown in Section 4.

2 PATH-FOLLOWING CONTROL AND PROBLEM DEFINITION

First of all, let us introduce the autonomous control scheme for the agricultural tractor shown in Figure 1. We here consider a simple path-following control scheme, where θ is the heading angle error, L_d is the lateral error with respect to the path, and L is the look ahead length. More specifically, L is defined as the distance between the current position of the machine and a specific point on the reference path, named "look-ahead point". By choosing a constant value of L, the look-ahead point can be computed accordingly as shown in (Samuel et al, 2016). Therefore, the target steering angle δ_r can be defined as:

$$\delta_r = \theta + \sin^{-1}(L_d/L) \quad (1)$$

For the sake of clarity, the reference path is defined in advance on the basis of several specifications provided by farmer (namely the geometry of the field, the kind of implement, the size of the tractor, etc.).

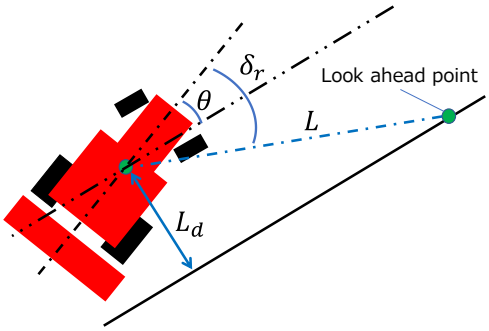

Figure 1: Autonomous control scheme.

Please notice that, at this stage, the controller does not take into account any disturbance. Therefore, it is not able to guarantee adequate motion accuracy while working on the agricultural field. In order to solve this problem a DOB is introduced, leading to the architecture displayed in Figure 2, where d is disturbance used for compensation.

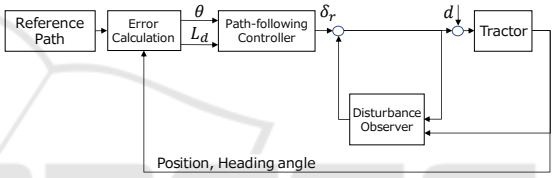

Figure 2: Block diagram of closed loop system.

3 DISTURBANCE OBSERVER DESIGN

We describe the tractor kinematics using the single-track model shown in Figure 3, where, a and b are the distances from the center of gravity position (CoG) to the front and rear wheel axle. v_y is the lateral velocity, V is the linear vehicle velocity, and δ is the steering angle.

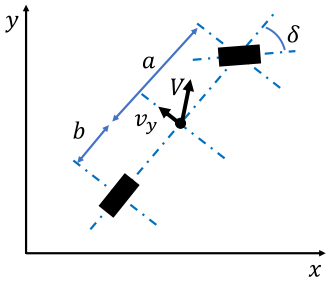

Figure 3: Single-track model.

The linearized single-track model is described as follows:

$$\dot{\mathbf{x}} = \mathbf{A}\mathbf{x} + \mathbf{B}u, \quad \mathbf{y} = \mathbf{C}\mathbf{x} \tag{2}$$

where $\mathbf{x} = [v_y \quad \omega]^t$ is the state variables vector, ω is the angular velocity, and $u = \delta$ is the control input. $\boldsymbol{A} \in \boldsymbol{R^{2,2}}$ is the state matrix, $\boldsymbol{B} \in \boldsymbol{R^{2,1}}$ is the input matrix, and $\boldsymbol{C} = I_2$ is the output matrix. **A** and **B** are given as follows:

$$\mathbf{A} = \begin{bmatrix} \frac{(-K_f - K_r)}{mV} & \frac{(-mV^2 - aK_f + bK_r)}{mV} \\ \frac{(-aK_f + bK_r)}{IV} & \frac{(-a^2K_f - b^2K_r)}{IV} \end{bmatrix} \tag{3}$$

$$\mathbf{B} = \begin{bmatrix} \frac{K_f}{m} & \frac{aK_f}{I} \end{bmatrix}^t \tag{4}$$

where K_f and K_r are the front and rear cornering forces, m is the vehicle mass, and I is the vehicle moment of inertia around the vertical axis. It is worth noticing that the dynamics induced by the relaxation length of the tires (Werner, 2015) has not been considered, since the introduction of the DOB will compensate the phenomena. Moving back to the model, the transfer functions $G_1(s)$, between δ and v_y and $G_2(s)$, between δ and ω, can be easily retrieved by combining equations (2), (3) and (4).

As a consequence, the target steering angle can be estimated from G_1^{-1} and G_2^{-1} by using the measured angular velocity and lateral velocity. Given the estimation of the steering angle, the DOB is able to compensate external disturbances acting on the control variable. The overall scheme is shown in Figure 4, where Q represents the filter belonging to the DOB to realize the invention, u_r is the control input provided by the path following controller, $\hat{\delta}$ is the estimation of the disturbance, d is an external disturbance acting on the steering angle, G_{t1} and G_{t2} are tractor's actual transfer function between lateral velocity / angular velocity and steering angle respectively, and K_1 and K_2 are the controller gains, whose tuning strategy will be discussed later.

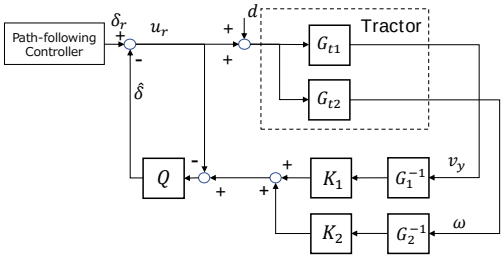

Figure 4: Block diagram of disturbance observer.

3.1 DOB Analysis

In this subsection the relevant properties of DOB will be discussed. Let's consider the closed loop system, shown in Figure 4. In this case the following relationships hold in the frequency domain:

$$v_y = G_{t1}(u_r + d), \omega = G_{t2}(u_r + d). \tag{5}$$

$$u_r = \delta_r - \hat{\delta}. \tag{6}$$

By using the well-known block schemes rules it is possible to express the DOB output $\hat{\delta}$ as follows when $Q(s) \to 1$:

$$\hat{\delta} = K_1 G_1^{-1} v_y + (K_2 G_2^{-1} - G_{t2}^{-1})\omega + d \tag{7}$$

By combining equation (5), (6) and (7), we obtain,

$$\omega = G_{t2}(\delta_r - K_1 G_1^{-1} v_y - (K_2 G_2^{-1} - G_{t2}^{-1})\omega) \tag{8}$$

and, finally:

$$K_1 G_1^{-1} v_y + K_2 G_2^{-1} \omega = \delta_r \tag{9}$$

From this result two important properties of DOB are derived:

- the outputs of the closed loop system (v_y, ω) are independent from d. As a consequence, we can conclude that the proposed algorithm is able to compensate disturbances acting on the steering angle;
- the closed loop transfer functions are mainly described by G_1 and G_2. This means that the path following controller can be tuned by considering the nominal model.

3.2 Control Gains Tuning

In this subsection a method for the choice of K_1 and K_2 will be proposed. In particular, their choice is based on the idea of minimizing the effect of constant forces on the lateral position of the vehicle. The system is described by the following equation, when some external lateral force is applied to the tractor:

$$\dot{\mathbf{x}} = \mathbf{A}\mathbf{x} + \mathbf{B}u + \mathbf{M}f, \qquad \mathbf{y} = \mathbf{C}\mathbf{x} \tag{10}$$

where f is an external lateral force and **M** is given as follows:

$$\mathbf{M} = \begin{bmatrix} \frac{1}{m} & \frac{l_d}{I} \end{bmatrix}^t \tag{11}$$

where l_d is the point of application of the force respect to the CoG position.

Figure 5 shows the overall block scheme, $F_{t1}$and F_{t2} are the transfer functions between the force and the lateral velocity / angular velocity.

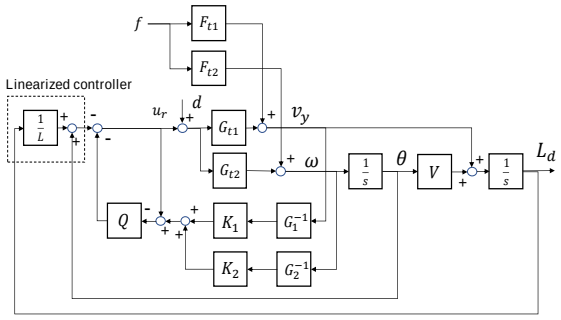

Figure 5: Block diagram under lateral force.

In order to facilitate the stability analysis of the system, the path-following controller defined in Equation (1) and the lateral error relationship have been linearized:

$$L_d \approx V\theta + v_y \tag{12}$$

$$\delta_r \approx \theta + L_d/L \tag{13}$$

By analysing the block scheme, the transfer function between the lateral error and the external lateral force, by setting to zero its static gain and considering:

$$\mathrm{Q} \approx 1, \qquad K_1 + K_2 = 1 \tag{14}$$

the following formulas can be retrieved:

$$\begin{aligned} K_1 &= G_1(0) \\ K_2 &= 1 - K_1 \end{aligned} \tag{15}$$

As it can be observed from Equation (15), not only the optimal gains depend solely on the nominal model, but they are also independent from both the point of application of the force (l_d), and its magnitude. This result is of particular interest for a practical implementation of the algorithm, since lateral forces are hardly ever measured in a real scenario.

3.3 Low Pass Filter Choice

The choice of a proper low pass filter Q is an important task in DoB design. As a matter of fact, this component is responsible of reducing the negative effects of high frequency measurement noises and ensuring the robust stability of the closed-loop system against unknown model parameters (Nguyen et al, 2014). To this scope, Q has been designed by considering the model uncertainties as multiplicative terms, represented in Equation (16) as:

$$G_{ti} = G_i(1 + \Delta G_i), \qquad i = 1,2 \tag{16}$$

By exploiting the small gain theorem, the following sufficient condition, that guarantees the input/output stability of the system, has been retrieved:

$$\|Q(\Delta G_1 k_1 + \Delta G_2 k_2)\|_\infty < 1 \tag{17}$$

thus leading to:

$$|Q(j\omega)| < |\Delta G_1(j\omega)k_1 + \Delta G_2(j\omega)k_2|^{-1}, \quad \forall\omega \geq 0 \tag{18}$$

This condition has finally been used to design the low-pass filter.

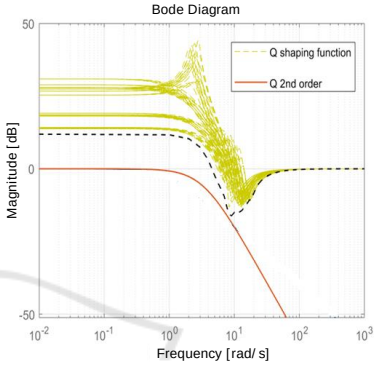

Figure 6: Frequency constraints imposed on the low-pass filter.

Figure 6 shows the shaping functions, represented by Equation (18), evaluated from a set of plausible parameters, and a possible filter's candidate.
A second order low-pass filter with a cut-off frequency of 0.53 Hz has been chosen in order to meet the above constraint in the worst-case scenario:

4 SIMULATION RESULTS

In order to test our proposed control architecture, a dynamic model of the tractor has been realized using the MATLAB/Simulink environment. This model has been developed according to (MathWorks, 2018) and (Narby, 2006), and it includes the dynamics of the vehicle body, the dynamics of the wheels, and also the tire relaxation model (Werner, 2015) needed to compute longitudinal and lateral forces. We develop the model as time-continuous model. Table 1 shows all the relevant parameters of the tractor model.

Table 1: Simulation parameters.

Parameter	Value
Vehicle mass (m)	4203.6 kg
Moment of Inertia (I)	2416.0 kgm2
Normarized lateral front tire stiffness (C_{yf})	4.18 1/rad
Normarized lateral real tire stiffness (C_{yr})	1.5469 1/rad
Distance between CoG and front tire axle(a)	1.67 m
Distance between CoG and rear tire axle(b)	0.73 m

In addition, the tire cornering force is calculated as follows:

$$K_f = \frac{C_{yf} m b}{(a+b)g}, \qquad K_r = \frac{C_{yf} m a}{(a+b)g} \tag{19}$$

where g represents the gravity acceleration.

The effectiveness of our control algorithm has been proved by considering three different simulation scenarios: plowing, moving on inclined field and moving in presence of significant sensor noise.

During plowing operations, the implement pulls the tractor and its asymmetrical structure exerts a lateral force on the vehicle, as it is shown in Figure 8.

In order to simulate the effect of the external forces exerted by the implement, load data measured during previous experiments have been used as reference. For the sake of completeness, a load cell was installed on the implement's attachment and forces were acquired during working.

Given the fact that agricultural tractors usually work at constant speed, we considered the vehicle moving at 3.00 km/h on a straight path with a look ahead distance of 4.00 m. Then, we input the external force to the tractor as a step disturbance.

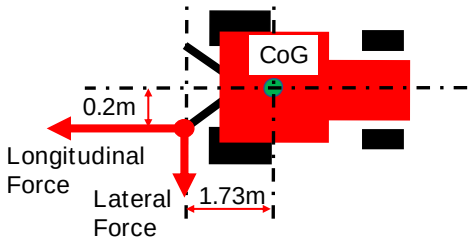

Figure 7: Plowing simulation.

The external force is activated at 30.00 sec from the simulation start. The force value was set to 23000.00N for longitudinal direction, 2000.00 N for lateral direction. We here provide the results of three different simulations. During the first one, the tractor is controlled by the path-following algorithm introduced in Section II. During the second one, the DOB discussed in Section III is introduced. CoG position is its correct nominal position (a =1.67 m, b = 0.73 m), and the optimal gains are computed according to Equations (15), under the 3.00 km/h velocity constraint, leading to the following values:

$$K_1 = 0.2381, \qquad K_2 = 0.7619$$

Finally, during the third simulation, the DOB is implemented by choosing a different nominal model with respect to the real system. As a matter of fact, the main property of DOB is the capability to force the system to behave like the nominal model. For this reason, if G_1 and G_2 are chosen properly it's possible to improve the dynamic performances of the closed-loop system. With such choice particular attention should be put into the stability analysis, since the mismatches between the nominal model and the real system will be much bigger.

Figure 8 (Figure 9) shows the Bode diagram of the transfer function between the steering angle δ and the lateral velocity v_y (angular velocity ω) with respect to different CoG position values. A bigger bandwidth is achieved for smaller values of a .

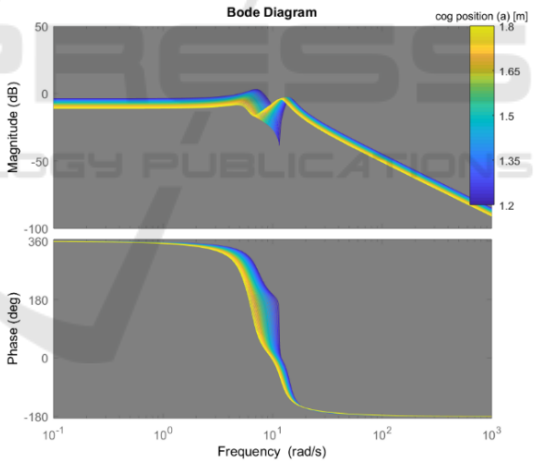

Figure 8: Bode diagram from δ to V_y with respect to CoG.

In order to speed up the system response, the nominal CoG position has been chosen closer to the front wheels (a = 0.1 m, b = 2.3 m). In this case, DOB gains are calculated as follows:

$$K_1 = 0.7891, \qquad K_2 = 0.2109.$$

The I/O stability is guaranteed by Equation (18) as it is shown by Figure 10.

Figure 11 shows the lateral errors corresponding to the three simulations. In absence of DOB, the controller is not able to reject the disturbance

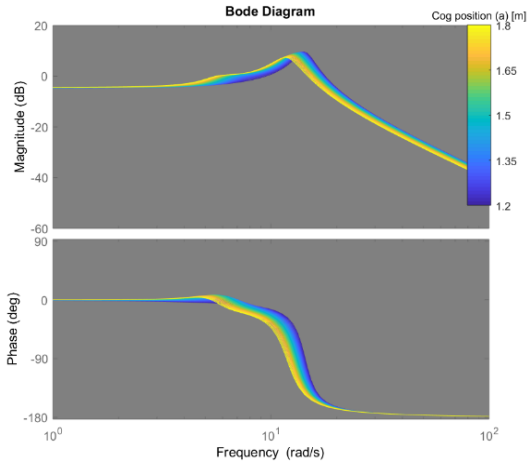

Figure 9: Bode diagram from δ to ω with respect to CoG.

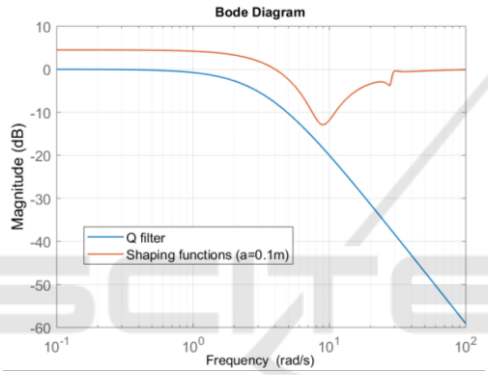

Figure 10: Frequency constraints imposed on the low-pass filter by choosing $a = 0.1$m.

originating from the external force. As a result, the lateral error rapidly increases and, more importantly, the steady-state lateral error at the end of the transient is not null. On the other hand, the controller endowed with the DOB is able to reject the external force as disturbance and to limit the lateral error. Moreover, by setting $a = 0.1$ the transient response is improved, but in the end, it converges to the same steady-state value as the DOB using the correct nominal model.

To further prove the superior performance of our approach, Table 2 shows the comparison among the three control architectures in terms of Root Mean Square Error (RMSE) and maximum error with respect to the predefined path.

Table 2: Simulation Results about lateral error.

Controller	RMSE	Maximum
Path-Following	5.17 cm	8.34 cm
Nominal DOB-based	1.59 cm	2.78 cm
Modified DOB-based	1.29 cm	2.02 cm

Finally, Figure 12 shows the heading angle with respect to the predefined path direction. Since we just control the steering angle, all the controllers reach a non-zero heading angle under the action of the external force. That said, once again the two controllers endowed with DOB (especially the one characterized by $a = 0.1$) demonstrate superior performance in terms of convergence time of the heading angle with respect to the default path-tracking controller.

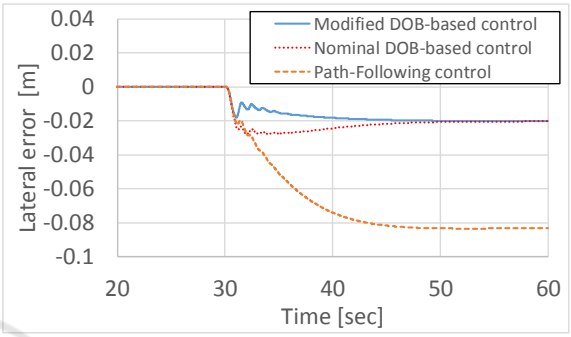

Figure 11: Lateral error of plowing scenario.

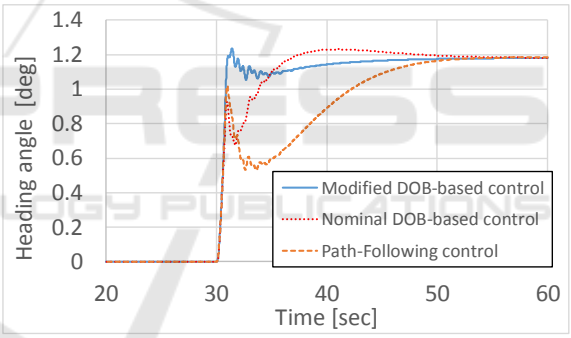

Figure 12: Heading angle of plowing scenario.

Moving to the second simulation scenario, we here consider the tractor moving on inclined ground. To properly simulate the effect of gravity on the inclined ground, a constant lateral force of acting on the CoG is considered. More in depth, the force value was set to 7000.00 N, since this value corresponds to the lateral component of the gravity force of the simulated tractor moving on a 10.00 degrees inclined field. Once again, the external force acts like a step disturbance that is activated at 30.00 sec from simulation start. Not differently from the previous scenario, we here consider the results of three different simulations: path-following control, nominal DOB-based control and modified DOB-based control. Figure 13 shows the lateral errors corresponding to the three simulations.

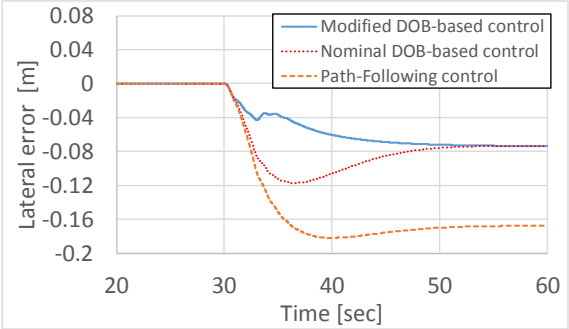

Figure 13: Lateral error of inclined scenario.

As far as RMSE and maximum error are concerned, Table 3 shows the comparison among the three controllers, further proving that our proposed architecture guarantees a significantly lower error with respect to the default path-following control.

Table 3: Simulation Results about lateral error.

Controller	RMSE	Maximum
Path-Following	11.44 cm	18.17 cm
Nominal DOB-based	6.10 cm	11.74 cm
Modified DOB-based	4.42 cm	7.37 cm

Finally, in the third simulation scenario we consider the motion in presence of significant sensor noise. In order to emulate this condition, we modify yaw rate and steering angle measurements. As far as the steering angle is concerned, the real value was edited by adding a random white noise with 1.00 degree offset and amplitude equal to 10% of the signal excursion. On the other hand, as far as the yaw-rate is regarded, the amplitude of the additive noise is equal to 1.00 degree/sec. The external force action is simulated in the same way as the plowing scenario and the simulation is repeated three times to collect the outputs of the three different control strategies. Figure 14 shows the lateral errors corresponding to the three simulations.

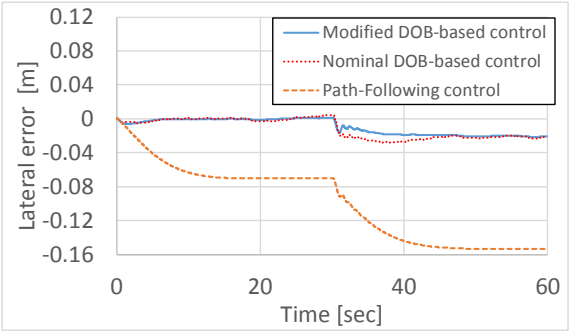

Figure 14: Lateral error of sensor noise scenario.

Clearly, in this scenario the default path-following controller is not able to counteract the effects of the steering offset, while the two DOB-based controllers successfully compensate it. Finally, Table 4 shows the comparison of the three control algorithms in terms of RMSE and maximum error.

Table 4: Simulation Results about lateral error.

Controller	RMSE	Maximum
Path-Following	10.92 cm	15.32 cm
Nominal DOB-based	1.61 cm	2.81 cm
Modified DOB-based	1.31 cm	2.15 cm

Given the fact that the typical desired motion accuracy is 5.00 cm (RMSE) and 10.00 cm (maximum), we can state that the proposed control algorithm is completely compliant with the imposed requirements.

5 CONCLUSIONS

In this paper, we propose a DOB-based path-following control algorithm able to improve the accuracy of an autonomous agricultural tractor in terms of lateral error with respect to a pre-defined path. The DOB was designed on the basis of the single-track vehicle model. The effectiveness of the proposed control architecture was tested in a simulation environment, considering three different scenarios: plowing, moving on inclined field and moving in presence of significant sensor noise. Results show that the proposed controller is able to reduce lateral error to 5 cm (RMSE) and 10 cm (maximum), among all the considered scenarios.

As far as future developments are concerned, we'll try to apply the same DOB-based control architecture to tracked vehicles, such as combine harvesters. Due to the fact that the kinematics of tracked vehicles does not allow to directly express the transfer function between the lateral velocity and the angular velocity of the vehicle, a different modelling approach will be considered, like for instance the one proposed in (Morita et al, 2018). On the other hands, an adaptive control scheme for the implementation of a DOB on tracked vehicles will also be considered. One possible approach regarding tracked mobile robot is proposed in (Hiramatsu et al, 2019). Finally, we will integrate these experience to the real agricultural vehicles.

REFERENCES

Ball, D., Ross, P., English, A., Milani, P., Richards, D., Bate, A., Upcraft, B., Wyeth, G., Corke, P., 2017. Farm

workers of the future. In *IEEEE Robotics & Automation Magazine*.

Blackmore, S., 2009. New concepts in agricultural automation. In *HGCA conference*.

Fang, H., Fan, R., Thuilot, B., Martinet, P., 2005. Trajectory tracking control of farm vehicles in presence of sliding, In *IEEE/RSJ International conference on Intelligent Robots and Systems*.

Hiramatsu, T., Morita, S., Pencelli, M., Niccolini, M., Ragaglia, M., Argiolas, A., 2019. Path-Tracking controller for tracked mobile robot on rough terrain, In *International conference on field and service robotics*.

Huang, D., Hai, J., 2015. Trajectory tracking control of wheeled mobile robots based on disturbance observer, In *IEEE Chinese Automation Congress.*

Hyungbo, S., Gyunghoon, P., Youngjun, J., Juhoon, B., Nam Hoon, J., 2016. Yet another tutorial of disturbance observer: robust stabilization and recovery of nominal performance. In *Control theory and technology. South China University of technology and academy of mathematics and systems science, vol. 14*.

Lenain, R., Thuilot, B., Cariou, C., Martinet, P., 2004. Adaptive and predictive nonlinear control for sliding vehicle guidance, In *IEEE/RSJ International conference on Intelligence Robots and Systems*.

MathWorks, 2018 Modeling a vehicle dynamics system, retrieved February 7, 2019 from https://jp.mathworks.com/help/ident/examples/modeling-a-vehicle-dynamics-system.html?lang=en.

Morita, S., Hiramatsu, T., Niccolini, M., Argiolas, A., Ragaglia, M., 2018. Kinematic track modelling for fast multiple body dynamics simulation of tracked vehicle robot, In *The 24th International Conference on Methods and Models in Automation and Robotics*.

Narby, E., 2006. Modeling and estimation of dynamics tire properties, In *examensarbete, Department of Electrical Engineering Linköpings tekniska högskola Linköpings universitet.*

Nguyen, B., M., Fujimoto, H., Hori Y., 2014. Yaw angle control for autonomous vehicle using Kalman filter based disturbance observer. In *SAEJ. EVTeC and APE Japan*.

Noguchi, N., Barawid Jr, O, C., 2011. Robot farming system using multiple robot tractors in Japan agriculture. In *18th IFAC world congress Milano*.

Pentzer, J., Brennan, S., Reichard, K., 2014. Model-based Prediction of Skid-steer Robot Kinematics Using Online Estimation of Track Instantaneous Centers of Rotation, In *Journal of Field Robotics*.

Rathgeber, C., Winkler, F., Odenthal, D., Muller, S., 2015. Disturbance observer for lateral trajectory tracking control for autonomous and cooperative driving. In *International journal of mechanics and mechatronics engineering vol. 9.*

Samuel, M., Hussein, M., Mohamad, B., Lucky, W., 2016. A review of some pure-pursuit based path tracking techniques for control of autonomous vehicles, In *International journal of computer applications.*

Shalal, N., Low, T., McCarthy, C., Hancock, N., 2013. A review of autonomous navigation systems in agricultural environments, In *SEAg 2013*.

Taghia, J., Katupitiya, J., 2013. A sliding mode controller with disturbance observer for a farm vehicle operating in the presence of wheel slip. In *IEEE/ASME international conference on advanced intelligent mechatronics*.

Wen-Hua, C., Jun, Y., Lei, G., Shihua, L., 2016. Disturbance-observer-based control and related methods – An overview. In *IEEE Transl. Industrial electronics., vol. 63.*

Werner, R., 2015. Centimeter-level accuracy path tracking control of tractors and activity steered implements. Ph.D. thesis, Technischen Universität Kaiserslautern zur Verleihung des akademischen Grades.

Yu, S., Wang, J., Wang, Y., Chen, H., 2018. Disturbance observer based control for four wheel steering vehicles with model reference. In *IEEE/CAA Journal of Automatica Sinica,*